Controlling Spatial Distributions of Molecules in Multicomponent Organic Crystals, with Quantitative Mapping by Confocal Raman Microspectrometry

Benjamin A. Palmer,[†] Annaïg Le Comte,[†] Kenneth D.M. Harris,*,[†] and François Guillaume*,[‡]

[†]School of Chemistry, Cardiff University, Park Place, Cardiff CF10 3AT, Wales
[‡]Groupe Spectroscopie Moleculaire, ISM, Université de Bordeaux I, UMR CNRS 5255, 33405 Talence Cedex, France

S *Supporting Information*

ABSTRACT: We report four experimental strategies for controlling the three-dimensional arrangement of molecules in multicomponent organic crystals, exploiting confocal Raman microspectrometry to quantify the three-dimensional spatial distributions. Specifically, we focus on controlling the distribution of two types of guest molecule in solid organic inclusion compounds to produce composite core−shell crystals, crystals with a homogeneous distribution of the components, crystals with continuous compositional variation from the core to the surface, and crystals with alternating shells of the components. In this context, confocal Raman microspectrometry is particularly advantageous over optical microscopy as it is nondestructive, offers micrometric spatial resolution, and relies only on the component molecules having different vibrational properties.

Multicomponent crystals or cocrystals[1] are important in the pharmaceutical industry[2] and have the potential to be used as advanced functional materials, exhibiting new optical,[3] electronic, and magnetic[4] properties. Many of these materials are based on the concept of isostructurality, whereby the chemically distinct subunits in the composite solid adopt very similar packing arrangements. It is particularly attractive to "tailor" the function of such materials simply by varying the spatial distribution of the components in the material,[3,4] while maintaining the same crystal structure. Such multicomponent crystals span a wide range of chemical types from metal alloys[5] to hybrid inorganic/organic systems,[6] organic solid solutions,[7] and crystals resulting from dyeing/zoning procedures.[8] Recently, metal organic frameworks (MOFs) containing mixtures of components have also attracted attention in view of their potential as tunable multifunctional materials. Such mixed MOF crystals may be constructed either by altering the metal center[3,4,9a−c] and keeping the organic linker constant or by altering the organic linker and keeping the metal center constant.[9d−g] Strategies to synthesize mixed MOFs have generated composite core−shell crystals[3,4,9a−f] and solid solutions.[3,4,9f,g] Although the literature is replete with examples of mixed MOFs, there are far fewer examples of purely organic multicomponent crystals with controlled spatial distributions (e.g., core−shell arrangements[10]). With a few notable exceptions,[11] most studies of multicomponent crystals have relied heavily on optical microscopy to establish the spatial distribution of the components. However, this technique is limited by the requirement that the components have different optical properties, which may be particularly problematic for purely organic materials. Furthermore, this technique often requires the crystal to be cut prior to analysis.

Given these issues, we were motivated to develop ways of controlling the spatial distribution of components in purely organic multicomponent crystals and to demonstrate the advantages of using confocal Raman microspectrometry to quantify the three-dimensional spatial distribution of the components. Here we present four strategies for controlling the spatial distribution of guest molecules in solid organic inclusion compounds containing binary mixtures of guest molecules, including the formation of composite core−shell crystals, crystals with a homogeneous distribution of the components, crystals with continuous compositional variation from the core to the surface, and crystals with alternating shells of the components.

The specific inclusion compounds used as model systems for this work are urea inclusion compounds,[12] in which guest molecules (typically based on *n*-alkanes) are located within the one-dimensional tunnels (Figure 1a) of a crystalline urea host structure.[13] The guest molecules are densely packed along the host tunnels (diameter[13c] *ca.* 5.5 Å) with a periodic repeat that is usually incommensurate[13b,14] with the periodic repeat of the host
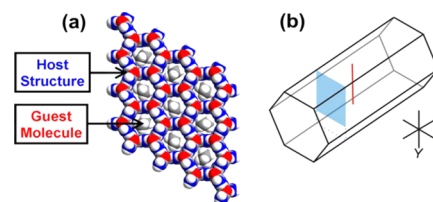

Figure 1. (a) Crystal structure of the hexadecane/urea inclusion compound viewed along the tunnel axis. (b) Schematic of a single crystal of a urea inclusion compound (needle morphology with hexagonal cross-section) with axis system defined. The Z-axis is parallel to the tunnel direction; the {100} faces are parallel to this axis. In the confocal Raman microspectrometry experiments, the incident laser was parallel to the Y-axis. Different types of mapping are indicated (red line, Y-scan; blue plane, XY-scan).
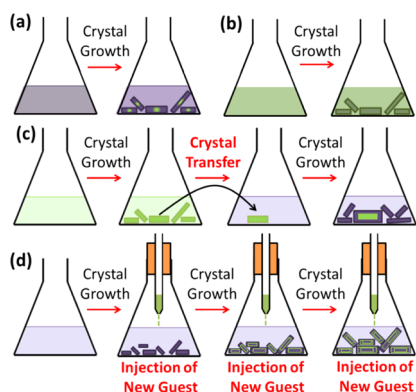
Figure 2. The four different crystal growth strategies to control the spatial distribution of guest molecules: (a) natural growth, (b) homogeneous growth, (c) transfer method, and (d) injection method.

structure. For urea inclusion compounds containing binary mixtures of guest molecules, the host tunnel structure is independent of the relative proportions of the two types of guest and the material grows as a single crystal even though the guest composition inside the crystal may vary. Some of the strategies presented here rely on the fact that different guest molecules have different relative affinities for inclusion within the host tunnel structure.[15] Specifically, under conditions of competitive co-inclusion from a crystallization solution containing a binary mixture of guest molecules, the molar ratio of guest molecules incorporated at the growing surfaces of the crystal at time t is $m_A(t) = \chi \gamma_A(t)$, where χ depends on the relative affinity of the host tunnel for inclusion of guests of types A and B and $\gamma_A(t)$ is the molar ratio of the guest molecules in the crystallization solution. If inclusion of guests of type A is energetically favored over inclusion of guests of type B, then $\chi > 1$ and hence $m_A(t) > \gamma_A(t)$.

One of the four strategies for controlling the spatial distribution of components reported here—the *natural growth* strategy (Figure 2a)—has been discussed previously,[16] and involves crystal growth under conditions of competitive co-inclusion of two different types of guest (denoted A and B). If the relative affinity of incorporating guest A into the crystal is higher than that for guest B (i.e., $\chi > 1$), then the initial stages of growth are dominated by incorporation of guest A. As a consequence, guest A is depleted from the solution more rapidly than guest B [i.e., $\gamma_A(t)$ decreases with time]; hence, as crystallization proceeds, the proportion of guest A incorporated into the crystal decreases [from the equation $m_A(t) = \chi \gamma_A(t)$, if $\gamma_A(t)$ decreases with time, then $m_A(t)$ also decreases with time]. This process leads to a monotonic variation in the composition of the crystal: the region with the highest proportion of guests of type A corresponds to the earliest stages of growth and the region with the lowest proportion of guests of type A corresponds to the latest stages of growth (Figure 3a).
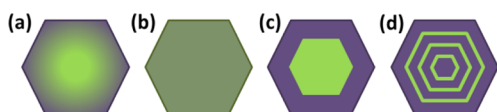

Figure 3. Schematic representations of the types of mixed crystals produced from the crystallization strategies in Figure 2, with different spatial distributions of guest molecules: (a) natural growth, (b) homogeneous growth, (c) transfer method, and (d) injection method.

In *homogeneous growth* (Figure 2b), the crystal is grown from a solution containing a mixture of two types of guest that have essentially equal affinity to be included in the crystal (i.e., $\chi \approx 1$). In this case, the ratio of the two types of guest in the crystal should be the same as the ratio in the crystallization solution [i.e., $m_A(t) \approx \gamma_A(t)$] and remains essentially constant during crystal growth. The resultant crystal should contain a homogeneous spatial distribution of the two types of guest in the same ratio as the initial crystallization solution (Figure 3b).

In the *transfer method* (Figure 2c), a seed crystal is grown in a solution containing one type of guest (A) and then transferred to a second crystallization solution containing a different type of guest (B).[17] The resultant crystal is expected to contain discrete regions with only guest A in the inner core and only guest B in the outer shell (Figure 3c). In principle, the crystal could be transferred multiple times between different crystal growth solutions (involving two or more different types of guest) to produce different generations of heterogeneous composite crystal with sequences such as AB, ABA, ABAB, ABC, etc.

In the *injection method* (Figure 2d), crystallization begins with a single type of guest (B) in solution. After the first crystals of the inclusion compound appear, small aliquots of a different guest (A) are injected at regular time intervals into the solution. Guest A is selected as one with a significantly higher affinity for incorporation into the growing crystal. Hence, although present in a relatively small proportion in the crystallization solution, guest A is the predominant guest incorporated into the crystal in the period immediately following injection. Shortly thereafter, all the injected guest A is consumed and guest B again dominates the crystal growth until the next injection of guest A. The resultant crystal should comprise mainly guest B, but with "bands" rich in guest A associated with each injection (Figure 3d). As the time between injections is known, the "bands" rich in guest A act as time-markers, and analysis of the distribution of these bands within the final crystal could potentially be exploited to yield kinetic information on the crystal growth process.

In all experiments discussed in the following sections, the two types of guest were an α,ω-dibromoalkane and an alkane, recognizing that the different Raman signatures of these molecules allow their spatial distribution in the crystals to be determined readily by confocal Raman microspectrometry. In the natural growth and transfer method experiments, the guests were 1,8-dibromooctane (1,8-DBrO) and pentadecane (PD). For homogeneous growth, 1,8-DBrO and undecane (UD) were used, and for the injection method, 1,8-DBrO and hexadecane (HD) were used. The affinity of the urea host structure for including PD and HD guests is significantly greater than that for 1,8-DBrO, whereas UD and 1,8-DBrO have essentially equal affinities for inclusion (and thus are appropriate for the homogeneous growth experiment).

After crystallization, a single crystal was selected and the guest composition was determined as a function of position in the crystal using confocal Raman microspectrometry. Previous studies[18] (with a different motivation) demonstrated that the spatial distributions of alkane and α,ω-dibromoalkane guests in urea inclusion compounds are readily quantified using this technique. Specifically,[19] the quantity R_N established from analysis of the Raman micrographs indicates the relative amounts of α,ω-dibromoalkane and alkane guests as a function of three-dimensional position in the crystal. Higher R_N indicates a higher proportion of α,ω-dibromoalkane. By definition, $0 \leq R_N \leq 1$, with the limiting values being attained when only the α,ω-dibromoalkane ($R_N = 1$) or only the alkane ($R_N = 0$) is present.
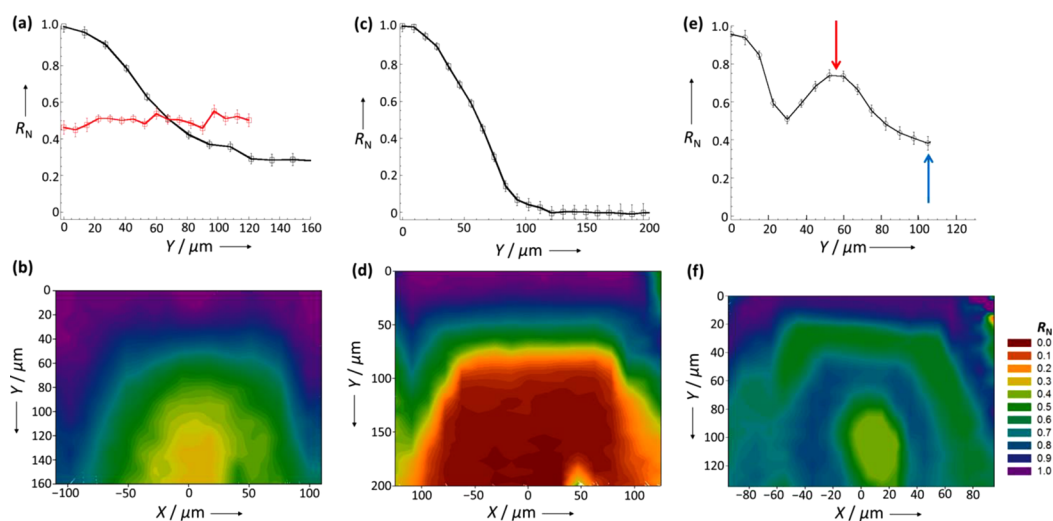
Figure 4. (a) *Y*-scans for crystals produced by natural growth (black) and homogeneous growth (red) [total thickness of crystals along *Y*-axis: 250 μm (natural growth), 205 μm (homogeneous growth)], and (b) *XY*-scan for the crystal prepared by natural growth. (c) *Y*-scan and (d) *XY*-scan for a crystal produced by the transfer method (total thickness of crystal along *Y*-axis: 415 μm). (e) *Y*-scan and (f) *XY*-scan for a crystal produced by the injection method (total thickness of crystal along *Y*-axis: 220 μm). The color scheme for values of R_N is defined in the inset.

The crystal morphology of conventional urea inclusion compounds is long needles with hexagonal cross-section (Figure 1b). The host tunnels are parallel to the needle axis (*Z*-axis). Analysis by confocal Raman microspectrometry involved one-dimensional "*Y*-scans" (with *X* and *Z* fixed) or two-dimensional "*XY*-scans" (with *Z* fixed at *Z* = 0 μm) within the crystal as depicted in Figure 1b. The incident laser was parallel to the *Y*-axis and *Y* = 0 μm represents the upper surface of the crystal. Along the *Y*-axis, the scans reported here typically extended from the upper surface to a region near the center of the crystal.

Figure 4a shows results from *Y*-scans for crystals produced by natural growth and homogeneous growth. In each case, the crystal contains both types of guest molecule, but with a substantial difference in the spatial distribution. In the case of natural growth, R_N varies continuously and monotonically as a function of depth on moving from the center of the crystal ($R_N \approx$ 0.3; rich in PD guests) to the surface ($R_N \approx$ 1.0; essentially only 1,8-DBrO guests). The observed variation of R_N as a function of depth is entirely consistent with the expectation that the region around the center of the crystal ($X \approx 0$ μm; $Y \approx 140$ μm) was formed at the earliest stage (i.e., lowest R_N) and the regions near the surface ($Y = 0$ μm) were formed at the latest stage (highest R_N) of the crystal growth process. These observations are consolidated by the results of two-dimensional *XY*-scans (in a plane perpendicular to the tunnel direction). In the case of natural growth (Figure 4b), the variation of guest composition reveals the development of the hexagonal cross-section of the crystal shape, with essentially equal rates of growth of the symmetry-related {100} faces.

In the case of homogeneous growth, on the other hand, there is no significant variation in R_N as a function of depth (*Y*) in the crystal, with $R_N \approx 0.5$ throughout the crystal. The molar ratio of the two guests in the initial crystallization solution was 0.5, demonstrating that, as predicted above, the 1,8-DBrO/UD system is an example of a pair of guests for which the relative affinities for inclusion within the urea tunnel structure are essentially equal (i.e., $\chi \approx 1$).

For the crystal produced by the transfer method, the *Y*-scan (Figure 4c) exhibits some qualitative similarity to the *Y*-scan for the crystal prepared by natural growth (Figure 4a) in that R_N

increases monotonically from the interior of the crystal to the surface. However, for the crystal prepared by the transfer method, a large region (120 μm < *Y* < 200 μm) around the center of the crystal has R_N = 0, indicating that only PD guest molecules (the guest in the first crystallization solution) are present, whereas the region near the surface of the crystal (0 μm < *Y* < 20 μm) has R_N = 1, indicating that only 1,8-DBrO guest molecules (the guest in the second crystallization solution) are present. In the "intermediate region" (20 μm < *Y* < 120 μm), the rate of change of R_N from R_N = 0 to R_N = 1 as a function of *Y* is much greater than for the crystal produced by natural growth. The presence of both types of guest in this region (albeit in substantially varying relative amounts) arises because some amount of the first crystallization solution (containing PD molecules) was transferred together with the seed crystal to the second solution.[20] The central core originates from the PD/urea seed crystal grown in the original crystallization solution, while the 1,8-DBrO/urea shell in the outer region of the crystal arises from the post-transfer crystal growth. Optimization of the experimental procedure for the transfer method may allow the thickness of the intermediate region to be reduced, ideally to achieve an abrupt boundary between the core containing only PD guests and the shell containing only 1,8-DBrO guests. The two-dimensional *XY*-scan in Figure 4d confirms that the crystal produced from the transfer method exhibits the hexagonal cross-sectional shape at each stage of the growth process, with the well-defined PD core in the central region and the 1,8-DBrO shell near the surface.[21]

For the experiment using the injection method, the original crystallization solution contained 1,8-DBrO guest molecules (guest B), and a solution containing HD (guest A) was injected periodically as the crystal growth proceeded. From the *Y*-scan (Figure 4e), R_N fluctuates as a function of depth in the crystal, with minima at *Y* $\approx$ 30 and 105 μm, and maxima at *Y* $\approx$ 5 and 55 μm. The minima correspond to regions of the crystal that are relatively rich in HD, whereas the maxima correspond to regions relatively rich in 1,8-DBrO. The corresponding regions are also observed in the *XY*-scan (Figure 4f), in which two HD-rich regions (low R_N; green) and two 1,8-DBrO-rich regions (high R_N; blue/purple) are clearly identified. In the HD-rich regions,

growth occurred immediately following injection of HD into the crystallization solution,[22] and it is clear that the crystal actually started to grow immediately following the first injection of HD rather than in the period prior to the first injection (if crystal growth had started before the first injection, the core of the crystal would contain *only* 1,8-DBrO guests), as evidenced by the HD-rich region close to the center of the crystal ($X \approx 10\,\mu$m; $Y \approx 110\,\mu$m) and indicated by the blue arrow in Figure 2e. In the period following the first injection of HD, R_N increases with further growth, indicating that the HD introduced to the solution is consumed rapidly. Following the second injection of HD (30 min after the first injection), R_N drops rapidly as HD dominates the growth process again (indicated by the red arrow in Figure 2e). The fact that R_N does not drop abruptly (e.g., vertically in Figure 2e) immediately following the injection of HD suggests that, after injection, diffusion of HD molecules to the surfaces of the growing crystal is not instantaneous. These phenomena result in the formation of an "onionskin" crystal composed of shells that are alternately rich in the two types of guest molecule (see Figure 3d). However, for reasons discussed above, the composition of the crystal does not alternate abruptly between shells of only HD and shells of only 1,8-DBrO.

The results reported here demonstrate several successful experimental strategies that have been designed for controlling the spatial distribution of binary mixtures of guest molecules in solid organic inclusion compounds. In principle, these strategies could be applied to a wide range of materials, including any crystal constructed from two or more isostructural subunits, for instance other inclusion compounds such as gas hydrates, zeolites and other microporous inorganic solids, and metal−organic framework materials. This paper also demonstrates the utility of confocal Raman microspectrometry as a noninvasive and nondestructive technique for mapping the composition of multicomponent crystals. Although the interpretations in this paper have been restricted to a qualitative level, our ongoing research is focused on further optimizing the injection method to gain deeper kinetic insights into the crystal growth by using the "bands" as "time-markers" for the growth process. Current research is also directed toward understanding the physical properties of multicomponent crystals by investigating, *inter alia*, phase transition behavior and diffraction properties of solid inclusion compounds prepared with different types of spatial distribution of binary mixtures of guest molecules.

ASSOCIATED CONTENT

Ⓢ Supporting Information

Experimental procedures, typical Raman spectra, and more details on the quantification method. This material is available free of charge via the Internet at http://pubs.acs.org.

AUTHOR INFORMATION

Corresponding Author

HarrisKDM@cardiff.ac.uk; f.guillaume@ism.u-bordeaux1.fr

Notes

The authors declare no competing financial interest.

ACKNOWLEDGMENTS

REFERENCES

(1) Dunitz, J. D. *CrystEngComm.* **2003**, *5*, 506.
(2) Vishweshwar, P.; McMahon, J. A.; Bis, J. A.; Zaworotko, M. J. *J. Pharm. Sci.* **2006**, *95*, 499.
(3) MacDonald, J. C.; Dorrestein, P. C.; Pilley, M. M.; Foote, M. M.; Lundburg, J. L.; Henning, R. W.; Schultz, A. J.; Manson, J. L. *J. Am. Chem. Soc.* **2000**, *122*, 11692.
(4) Noveron, J. C.; Lah, M. S.; Del Sesto, R. E.; Arif, A. M.; Miller, J. S.; Stang, P. J. *J. Am. Chem. Soc.* **2002**, *124*, 6613.
(5) Kitaigorodsky, A. I. *Mixed Crystals*, Springer, Berlin, 1984.
(6) Férey, G. *Chem. Soc. Rev.* **2008**, *37*, 191.
(7) Mnyukh, Y. V. *Zh. Strukt. Khim.* **1960**, *1*, 370.
(8) (a) Kahr, B.; Gurney, R. W. *Chem. Rev.* **2001**, *101*, 893. (b) Bullard, T.; Wustholz, K. L.; Bott, E. D.; Robertson, M.; Reid, P. J.; Kahr, B. *Cryst. Growth Des.* **2009**, *9*, 982.
(9) (a) Dechambenoit, P.; Ferlay, S.; Kyritsakas, N.; Hosseini, M. W. *Chem. Commun.* **2009**, 1559. (b) Dechambenoit, P.; Ferlay, S.; Hosseini, M. W. *Cryst. Growth Des.* **2005**, 2310. (c) Ferlay, S.; Hosseini, M. W. *Chem. Commun.* **2004**, 788. (d) Furukawa, S.; Hirai, K.; Takashima, Y.; Nakagawa, K.; Kondo, M.; Tsuruoka, T.; Sakata, O.; Kitagawa, S. *Chem. Commun.* **2009**, 5097. (e) Yoo, Y.-S.; Jeong, H.-K. *Cryst. Growth Des.* **2010**, *10*, 1283. (f) Koh, K.; Wong-Foy, A. G.; Matzger, A. J. *Chem. Commun.* **2009**, 6162. (g) Koh, K.; Wong-Foy, A. G.; Matzger, A. J. *Angew. Chem., Int. Ed.* **2008**, *47*, 677.
(10) Bardelang, D.; Giorgi, M.; Pardanaud, C.; Hornebecq, V.; Rizzato, E.; Tordo, P.; Ouari, O. *Chem. Commun.* **2013**, *49*, 3519.
(11) (a) Olmsted, B. K.; Ferlay, S.; Dechambenoit, P.; Hosseini, M. W.; Ward, M. D. *Cryst. Growth Des.* **2009**, *9*, 2841. (b) Bres, E. F.; Ferlay, S.; Dechambenoit, P.; Leroux, H.; Hosseini, M. W.; Reyntjens, S. *J. Mater. Chem.* **2007**, *17*, 1559.
(12) (a) Hollingsworth, M. D.; Harris, K. D. M. *Comprehensive Supramol. Chem.*; (Eds: MacNicol, D. D.; Toda, F.; Bishop, R. Pergamon: Oxford, 1996; Vol. 6, pp 177−237. (b) Harris, K. D. M. *Supramol. Chem.* **2007**, *19*, 47.
(13) (a) Smith, A. E. *Acta Crystallogr.* **1952**, *5*, 224. (b) Harris, K. D. M.; Thomas, J. M. *J. Chem. Soc. Faraday Trans.* **1990**, *86*, 2985. (c) George, A. R.; Harris, K. D. M. *J. Mol. Graphics* **1995**, *13*, 138.
(14) (a) Rennie, A. J. O.; Harris, K. D. M. *Proc. R. Soc., London Ser. A* **1990**, *430*, 615. (b) Schmicker, D.; van Smaalen, S.; de Boer, J. L.; Haas, C.; Harris, K. D. M. *Phys. Rev. Lett.* **1995**, *74*, 734. (c) Lefort, R.; Etrillard, J.; Toudic, B.; Guillaume, F.; Breczewski, T. *Europhys. Lett.* **1998**, *43*, 546.
(15) (a) Harris, K. D. M.; Jupp, P. E. *Proc. R. Soc., London Ser. A* **1997**, *453*, 333. (b) Harris, K. D. M.; Jupp, P. E.; Lee, S.-O. *J. Chem. Phys.* **1999**, *111*, 9784.
(16) Palmer, B. A.; Harris, K. D. M.; Guillaume, F. *Angew. Chem., Int. Ed.* **2010**, *49*, 5096.
(17) More discussion of the transfer method is given in the SI.
(18) Marti-Rujas, J.; Desmedt, A.; Harris, K. D. M.; Guillaume, F. *J. Am. Chem. Soc.* **2004**, *126*, 11124.
(19) Quantitative analysis is focused on the C−Br stretching band ν(CBr) for the α,ω-dibromoalkane (650 cm^{-1} for the *trans* end-group conformation) and the symmetric C−N stretching band ν_s(CN) for urea (1024 cm^{-1}). Guest composition is established from the ratio $R = I$(CBr)$/I$(CN) of the integrated intensities of the ν(CBr) and ν_s(CN) bands, which is then normalized as $R_N = R/R_o$, where R_o is the value of R for the urea inclusion compound containing only the relevant α,ω-dibromoalkane (in this case 1,8-DBrO) as the guest. More details of the quantification method and representative Raman spectra are included in the SI.
(20) This issue is discussed further in the SI.
(21) The discontinuity observed in Figure 4d at $X = 50\,\mu$m, $Y = 200\,\mu$m is discussed in the SI.
(22) This assignment is consistent with the visual observation that many new crystals appeared in the solution following the first injection of HD, suggesting that crystal nucleation was actually triggered by the first introduction of HD into the solution.